Okhotsk Sea and Polar Oceans Research 2 (2018) 13-18

Article

Development of a new algorithm to estimate Arctic sea-ice thickness based on Advanced Microwave Scanning Radiometer 2 data

Kazutaka TATEYAMA[1], Jun INOUE[2], Seita HOSHINO[3], Shota SASAKI[1] and Yasuhiro TANAKA[1]

[1]*Kitami Institute of Technology, Kitami, Hokkaido, Japan*
[2]*Arctic Environment Research Center, National Institute of Polar Research, Tachikawa, Japan*
[3]*Graduate School of Engineering, Kitami Institute of Technology, Kitami, Hokkaido, Japan*

Abstract

Data from the Advanced Microwave Scanning Radiometer 2 (AMSR2) are used to evaluate the Arctic sea-ice thickness (SIT). The polarization ratio at 36 GHz (PR_{36}) and the gradient ratio between 6 and 36 GHz ($GR_{06\text{-}36}$), which contain the signals for the first-year ice and multi-year ice thicknesses, respectively, are used to estimate the draft of the sea-ice. The developed equation for the SIT is validated using SIT results derived from ice mass balance (IMB) buoys and the results are compared with the SIT data obtained from Cryosat-2 (CS2). For SIT calculations performed for the period from March to September, a seasonal bias correction was applied to the SIT that was derived from the AMSR2 algorithm based on the skin temperature, which was determined from an atmospheric reanalysis. This correction reduced the SIT error effectively; however, large errors that occur during the melting and refreezing season still remain because the existence of melt ponds and their refreezing affect the microwave radiation strongly. Improvement of the regional biases outside the validation area will be also necessary.

Key words: sea-ice thickness, passive microwave radiometer, AMSR2, Cryosat-2, ice mass balance buoy

(Received October 4, 2017; Revised manuscript accepted January 18, 2018)

1. INTRODUCTION

The annual to decadal variability of the Arctic sea-ice volume is highly relevant for evaluation of the Arctic fresh water budget and global climate change. The extent of the Arctic sea-ice has been monitored continuously using satellite-borne passive microwave radiometers such as the Scanning Multichannel Microwave Radiometer (SMMR) and the Special Sensor Microwave Imager (SSM/I) since the late 1970s (Comiso *et al*., 2008). However, acquiring observations of changes in the ice thickness has been challenging, and several approaches have been used to date. For example, the thin sea-ice thickness (SIT) with no snow has been provided by satellite-borne visible and infrared radiometers (Yu and Rothrock, 1996; Drucker *et al*., 2003) and passive and active microwave sensors (Kwok *et al.*, 1999, Giles *et al*., 2008; Tamura *et al*., 2008). Recently, a thick SIT algorithm was developed using altimeter data from both ICESat (e.g., Kwok *et al.*, 2007) and Cryosat-2 (e.g., Laxon *et al.*, 2013). However, these altimeters provide the ice thickness distributions monthly and weekly, but not daily.

A daily sea-ice draft estimation algorithm was developed for the Advanced Microwave Scanning Radiometer-EOS (AMSR-E), which was onboard the Earth Observing Satellite Aqua of the U.S. National Aeronautics and Space Administration (NASA); Aqua was launched in 2002, but stopped rotating in 2011. The algorithm was devised on the basis of in situ sea-ice draft data that were derived from upward looking sonar (ULS) devices mounted on mooring buoys in the Beaufort Gyre. These buoys have been located in the southern Canada basin since 2002 (Krishfield *et al.*, 2014). While the algorithm is corrected for seasonal errors using statistical methods, major underestimations occur in spring and summer.

In this study, the AMSR-E thickness algorithm was applied to data from a new microwave radiometer: the Advanced Microwave Scanning Radiometer 2 (AMSR2), located onboard the Earth observation satellite Global Change Observation Mission-Water (GCOM-W) of the Japan Aerospace Exploration Agency (JAXA), which was launched in 2012. Here, we evaluate the SIT values derived from the AMSR2 data and compare them with the in situ thicknesses derived from drifting buoys and other satellite sensors.

2. DATA AND METHOD

We used the brightness temperature (*TB*), which is observed twice a day by AMSR2 and provided at 10 km resolution in a polar stereographic projection from the JAXA, to calculate the sea-ice draft using the estimation algorithm that was developed for AMSR-E data (Krishfield *et al.*, 2014).

We evaluated the validity of the sea-ice draft thickness that was estimated from the AMSR2 data by comparing our results with the thicknesses measured using the satellite-borne altimeter that is mounted on Cryosat-2 (CS2) and in situ measurement results from ice mass balance (IMB) buoys.

2.1 Sea-ice draft algorithm

Cavalieri *et al.* (1984) defined the following sea-ice parameters: the gradient ratio (*GR*; Eq. 1) and the polarization ratio (*PR*; Eq. 2). These parameters are used to calculate ice concentrations for first-year (FY) ice and multi-year (MY) ice, respectively, as follows:

$$GR = \frac{TB_{\mathrm{V}} - TB'_{\mathrm{V}}}{TB_{\mathrm{V}} + TB'_{\mathrm{V}}} \quad (1)$$

$$PR = \frac{TB_{\mathrm{V}} - TB_{\mathrm{H}}}{TB_{\mathrm{V}} + TB_{\mathrm{H}}}. \quad (2)$$

Krishfield *et al.* (2014) suggested that the *PR* at 36 GHz (PR_{36}) and the *GR* in the range between 6 GHz and 36 GHz (GR_{06-36}) could be used to estimate the sea-ice drafts of FY ice and MY ice, respectively. They defined the sea-ice draft $D_{\mathrm{AMSR-E}}$ estimation formulae in the two equations below. When GR_{06-36} is greater than −0.035, the sea-ice type is regarded as FY ice, and Eq. 3 is used to estimate $D_{\mathrm{AMSR-E}}$:

$$\text{FY ice } D_{\mathrm{AMSR-E}}\,[\mathrm{m}] = 2.34\exp\left(\frac{PR_{36} - 0.0019}{0.0283}\right) + 0.085 \quad (3)$$

Conversely, when GR_{06-36} is less than −0.035, Eq. 4 is used to estimate $D_{\mathrm{AMSR-E}}$:

$$\text{MY ice } D_{\mathrm{AMSR-E}}\,[\mathrm{m}] = 0.244\exp(-20.785GR_{06-36}) + 0.162 \quad (4)$$

These formulae are based on in situ ice draft measurements from the ULS devices mounted on four mooring buoys from 2002 to 2011 in the Beaufort Sea; their locations are shown as stars in Fig. 1. In this context, the ice draft is the ice thickness below the waterline, while the ice freeboard is the ice thickness above the waterline. The SIT is generally defined as the total freeboard plus the ice draft.

A seasonal bias in the sea-ice draft derived from mooring buoys and AMSR-E data has been found (Krishfield *et al.*, 2014). This seasonal fluctuation is most likely to be caused by changes in the ice surface properties, such as melting during spring and summer, or snow during autumn and winter.

In this study, we applied the AMSR-E ice draft algorithm to AMSR2 data and validated the algorithm's effectiveness based on CS2 and IMB thicknesses.

2.2 Cryostat-2 thickness data

Monthly mean SIT data observed by the Synthetic Interferometric Radar Altimeter (SIRAL) onboard the CS2 satellite, which was launched by the European Space Agency in April 2010, were compared with the FY ice and MY ice draft thickness values estimated from the AMSR2 data. SIRAL is a microwave radar with a central frequency of 13.6 GHz that uses the K_U band to measure the sea-ice freeboard. The SIT can then be calculated from the freeboard value using the hydrostatic equilibrium (Laxon *et al.*, 2013).

We used the CS2 sea-ice freeboard, ice thickness, and snow depth data set projected on the EASE2.0 grid, which was provided by the Alfred Wegener Institute (Ricker *et al.*, 2014). This data set is available for the Arctic winter and spring seasons only, i.e., from October to May.

In this study, the monthly mean CS2 SIT and the monthly mean $D_{\mathrm{AMSR-E}}$ were compared at the locations shown in Fig. 1. Data sampling points were set at 85, 80, and 75°N and 0, 30, 60, 120, 135, 150, 165, 180°E and °W over the ice-covered area.

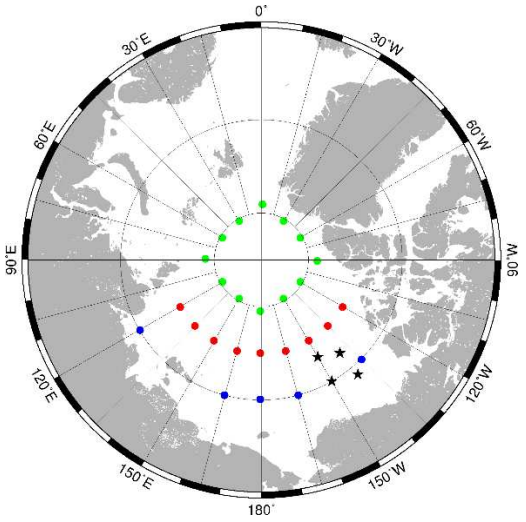

Fig. 1 Data sampling points for sea-ice draft and thickness located along 85°N (green), 80°N (red), and 75°N (blue). The stars and dots correspond to the daily sea-ice draft measurements based on ULS and AMSR2 data, respectively, during the period from 2002–2011 and the monthly mean CS2 derived SIT and AMSR2 sea-ice draft values from 2012 to 2013.

2.3 Ice mass balance buoy thickness data

The IMB buoys were deployed in the Arctic in 1993 and have provided datasets since 1993, which are available from the U.S. Army Engineer Research and Development Center's Cold Regions Research and

Engineering Laboratory. The IMB dataset contains hourly snow depth, ice thickness, sea-ice temperature profile, air temperature, barometric pressure, and ice drift data (see e.g., Richter-Menge *et al.*, 2006; Polashenski *et al.*, 2011).

The daily $D_{\mathrm{AMSR-E}}$ value was compared with the daily mean in situ SIT and the air and water temperatures, air pressure and snow depth measured by five IMB buoys during the period from 2012–2013. Fig. 2 shows the thickness distributions along the IMB tracks around the North Pole and the Canada basin.

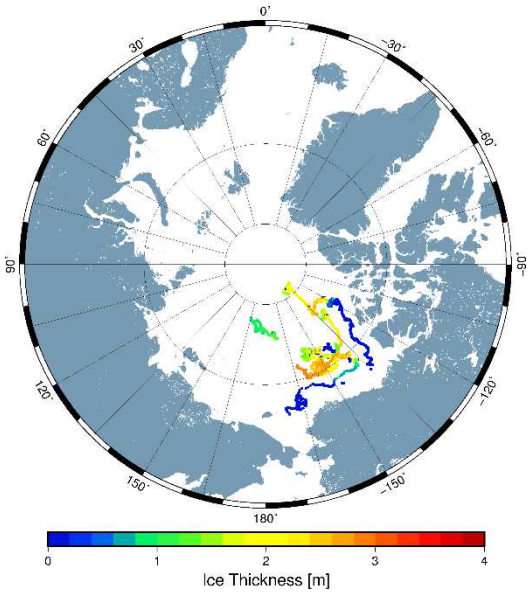

Fig. 2 SIT distributions along IMB tracks from 2012–2013.

3. RESULTS AND DISCUSSION

3.1 Comparison between CS2 thickness and AMSR2 draft

Figure 3 shows the results of our comparison between the monthly mean CS2 thicknesses and the AMSR2-derived draft using Krishfield's algorithm from October to May for 2012–2013. Figure 3a shows clear differences between the AMSR2 draft and the CS2 thickness along both the longitudinal and latitudinal ranges. There is an obvious regional bias that leads to a large underestimation in the western Arctic region related to the existence of MY ice and a relative overestimation in the eastern Arctic region related to Russian river discharges, which cause thicker sea-ice because of lower surface salinity over the ice surface.

Figure 3b shows seasonal variations in the AMSR2 draft and CS2 thickness along longitudes of 120°W, 180°E, and 120°E. Each longitude shows a seasonal bias, in which the AMSR2 data underestimate the draft towards the beginning of spring and show high scattering in autumn. Along 120°W, the AMSR draft tends to be underestimated throughout the year. The same underestimation appeared on 85 and 80°N but not on 75°N along 120°E. This seasonal bias probably reflects the high sensitivity of the microwave sensor to changes in sea-ice surface characteristics, particularly during the melting season from early spring to summer, and during the early stages of snow freezing on the melted surface. To identify the causes and improve the seasonal bias in the SIT, we compared in situ sea-ice surface changes.

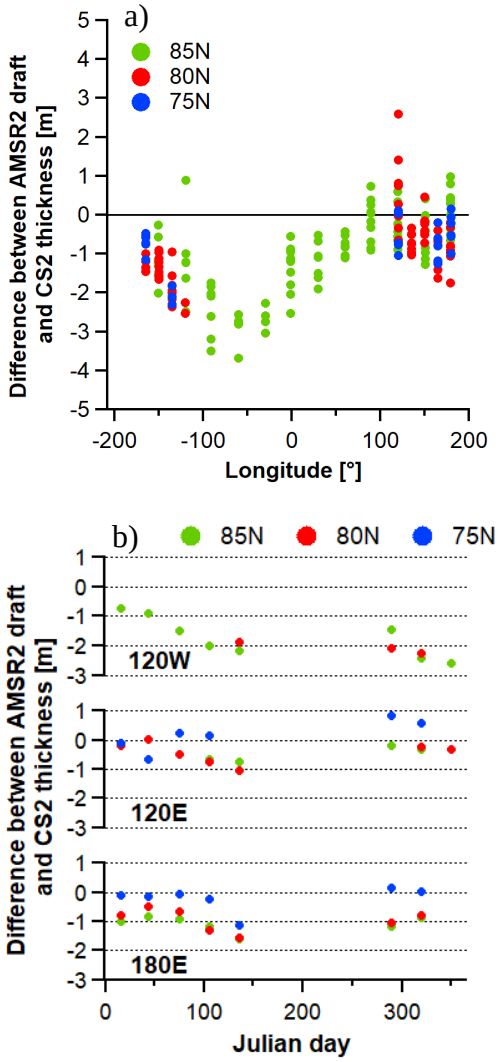

Fig. 3 Comparisons between monthly mean CS2 thickness and AMSR2 draft. a) Longitudinal cross-sections are along 85°N (green dots), 80°N (red dots), and 75°N (blue dots). Positive and negative longitudes mean East and West, respectively. b) Seasonal cross-sections along 120°W, 120°E, and180°E longitudes.

3.2 Comparison between IMB thickness, air temperature and AMSR2 draft

We analyzed the relationship between the AMSR2 draft and IMB SIT values to obtain a conversion formula from the AMSR2 draft D_{AMSR2} to the AMSR2 SIT H_{AMSR2}. The relationship between the IMB SIT

H_{IMB} and D_{AMSR2} values from September to February and their regression line are shown in Fig. 4. A conversion formula based on Fig. 4 is given as Eq. 5.

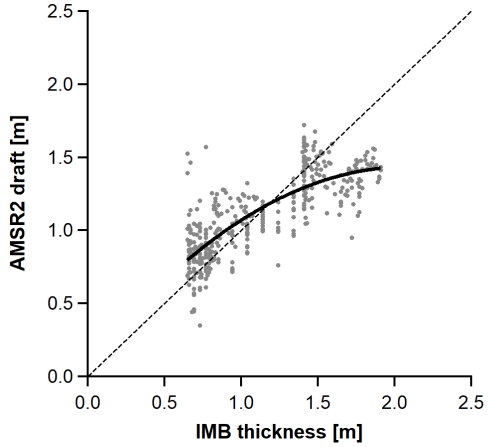

Fig. 4 Scatter diagram showing daily IMB SIT values for the five buoys shown in Fig. 2 versus the sea-ice draft estimated from AMSR2 data using Eq. 3 or 4.

Because the underestimation of the AMSR2 draft values increased over the period from winter to spring (Fig. 3d–f)), we investigated the differences in SIT values between H_{AMSR2} and H_{IMB} as a function of near-surface air temperature for all seasons (Fig. 5). The air temperature was closely correlated with the thickness difference between the values derived from AMSR2 and the IMB buoys. This indicates that there could be further improvements in the performance of the AMSR2 draft algorithm if a near-surface variable is used as a correction factor in Eq. 5.

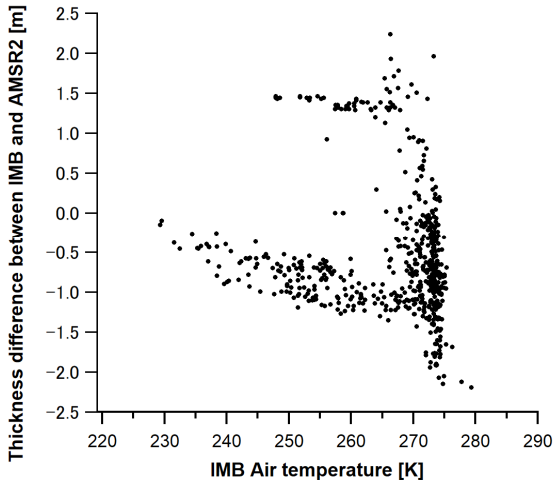

Fig. 5 Differences in thickness between IMB and AMSR2 methods, reflecting the effects of air temperature for both the autumn and winter data sets.

$$H_{\mathrm{AMSR2}}\ [\mathrm{m}] = 0.0477 + 0.821D_{\mathrm{AMSR2}} + 0.134{D_{\mathrm{AMSR2}}}^2 \quad (5)$$

However, because the air temperature data are obtained from drifting buoys over the Arctic Ocean, they are not generally assimilated into the reanalysis products, making them less useful for SIT estimation because of the large associated uncertainty. Instead, the skin temperature of the ice surface, which is determined using the surface heat budget, particularly the radiation balance from spring to autumn, is likely to be a more suitable parameter.

Figure 6a shows the relationship between the in situ air temperature derived from the IMB buoys and the skin temperature provided by the European Centre for Medium-Range Weather Forecasts (ECMWF) for 2012–2013. The skin temperature has a high correlation coefficient (R = 0.98 from March to May, with an annual value of R = 0.95).

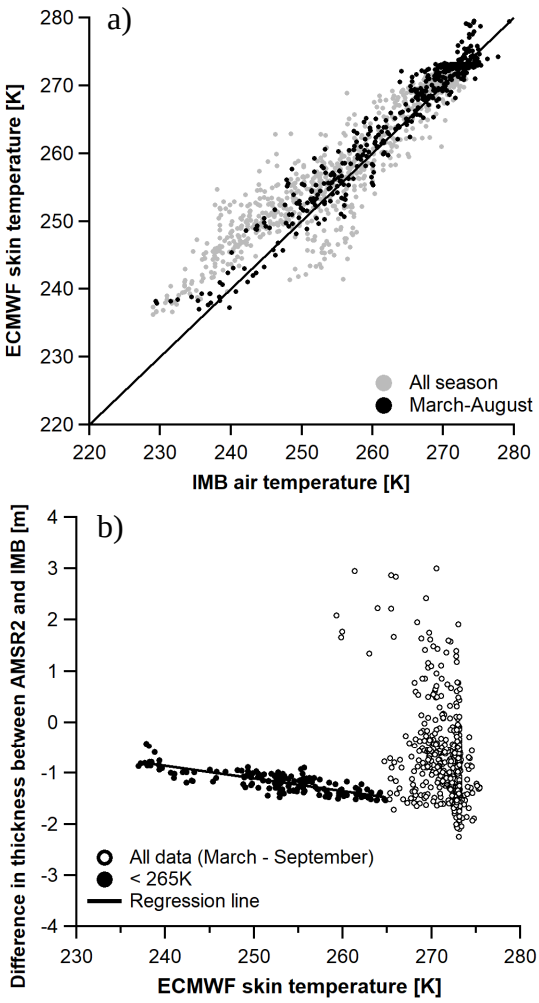

Fig. 6 a) Relationship between skin temperature provided by the ECMWF and in situ air temperature derived from the IMB, and b) the difference in SIT between the AMSR2 and IMB derivations during 2012–2013.

Figure 6b shows seasonal changes in skin temperature lower than 265 K (black dots) and the difference in thickness between H_{AMSR2} and H_{IMB} from March to September (gray dots). There is a systematic large difference in thickness as a function of skin temperature when it is lower than 265 K.

By focusing on temperatures of less than 265 K, the thickness deviation between H_{AMSR2} and H_{IMB} can be characterized as a linear function of the ECMWF skin temperature with a high correlation coefficient (R = –0.81). In this case, H_{AMSR2} can be corrected based on the skin temperature (T_{skin}) when it is lower than 265 K from March to September using Eq. 6.

$$H'_{\mathrm{AMSR2}}\ [\mathrm{m}] = H_{\mathrm{AMSR2}} - (5.07 - 0.0247T_{skin}) \quad (6)$$

We confirmed that Eq. 6 is valid for the period from March to September. While Krishfield *et al.* (2014) attempted to estimate the SIT over the Beaufort Sea using ULS observations, their equation still requires correction as a function of the Julian day to improve its empirical seasonal bias. The *TB* is a function of both temperature and emissivity (Cavalieri *et al.*, 1984). When the emissivity is constant, a change in skin temperature contributes to the *TB* change. This correction would be dependent on the latitude at which the in situ observations were made. In contrast, Eqs. 5 and 6 were generated from a larger area of the Arctic Ocean, which makes our algorithm more robust.

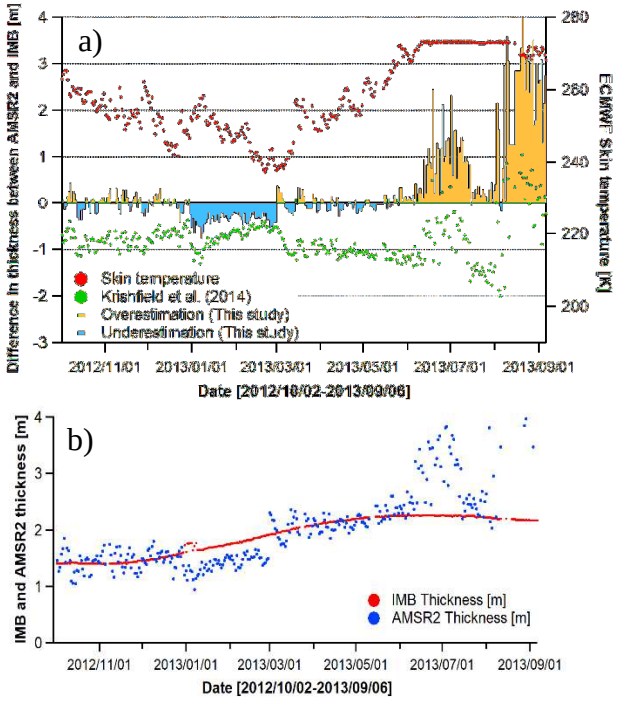

Fig. 7 Examples of skin temperature, differences in thicknesses between IMB and AMSR2 data and corrected AMSR2 draft values based on skin temperature in Eq. 6.

Finally, we investigated the validity of the H'_{AMSR2} values by comparing H'_{AMSR2} with H_{IMB}. Figure 7a shows an example of the relationships among skin temperature (red dots), and the SIT differences when determined using Krishfield's algorithm (green dots) and using the algorithm proposed here (blue and orange bars). The underestimation that was described previously for our algorithm increases as the skin temperature rises from March to June. Additionally, the large overestimates from June to September are likely to correspond to refreezing of melt ponds. The passive microwave radiometer is very sensitive to phase changes on the ice surface. This suggests that we could improve H_{AMSR2} estimates using the skin temperature during spring and autumn. The blue and orange bars in Fig. 7 show improvements related to skin temperature correction. Clearly, the thickness difference was minimized from March to June. Figure 7b shows better agreement between the IMB and AMSR2 results during the spring and summer seasons, suggesting that this modified algorithm provides more reliable SIT data for the spring and early summer periods.

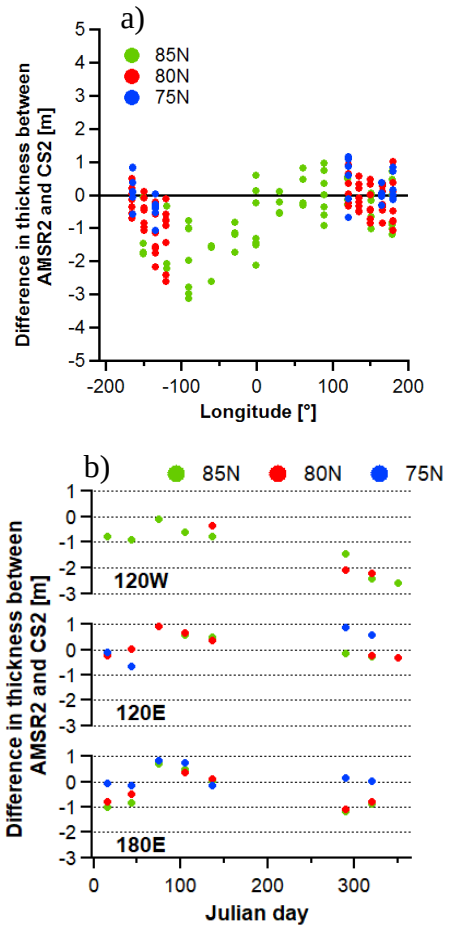

Fig. 8 Comparisons between monthly mean CS2 thickness and modified AMSR2 thickness along with the data of Fig. 3. a) Longitudinal cross-sections and b) seasonal cross-sections.

Comparisons between the monthly mean CS2 thickness and the modified AMSR2 thickness are shown in Fig.8. While a large underestimate remains in the western Arctic, the overall underestimated offset was improved using Eq. 5. The seasonal bias was also removed during the period from March to May.

Figure 9 shows an example of SITs estimated from AMSR2 data using a) Krishfield's algorithm and b) our improved SIT algorithm for 1 April 2013. Our improved SIT values are more than 2 m thick, which is approximately 1 m thicker than the values obtained using Krishfield's algorithm. This thicker ice area indicates thickness of more than 5 m in the north of Canadian Arctic Archipelago, which resembles the monthly CS2 SIT values in appearance.

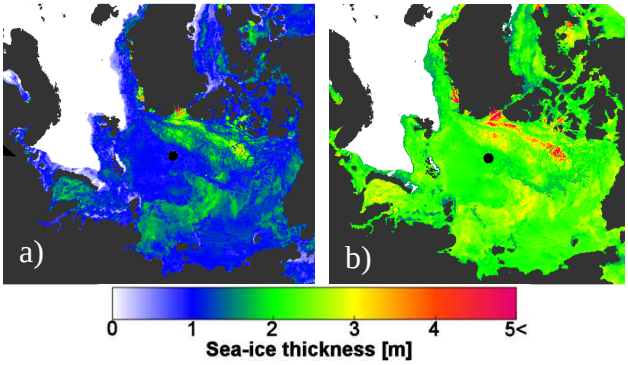

Fig. 9 Examples of AMSR2 SIT on April 1, 2013: a) with Julian day correction; b) with skin temperature correction.

4. CONCLUSIONS

A SIT algorithm for AMSR2 data was newly developed for the Arctic sea-ice in this study. The ice draft was estimated from AMSR2 data using an algorithm that was adapted from one designed for the AMSR-E data (Krishfield *et al.*, 2014). Ice draft values were converted to thicknesses by comparing them with the in situ thicknesses observed by IMB buoys from 2012 to 2013. The thickness differences among the CS2-, IMB- and AMSR2-based methods show seasonal variations because the microwave frequency is sensitive to phase changes on the ice surface. This seasonal bias was successfully minimized from March to June using the skin temperatures derived from the ECMWF. There also is a regional bias to the SIT estimates, in which SIT underestimation over the western Arctic is related to existence of MY ice. The algorithm was improved and validated within the Arctic Ocean via comparisons with CS2 and IMB data, as shown in Figs. 1 and 2. Therefore, there are overestimates of the SIT outside the validation area (e.g., Bering Sea, Sea of Okhotsk). Improvement of these regional biases is an issue for future work.

ACKNOWLEDGEMENTS

This study was supported by the Japanese Green Network of Excellence Program (GRENE), the Arctic Climate Changes Research Project, the Arctic Challenge for Sustainability Project (ArCS), and the Japan Society for the Promotion of Science (JSPS) Grants-in-Aid for Scientific Research (A) (grant no. JP26249133) and Scientific Research (C) (grant no. JP26340013). We are grateful to Dr. Richard Krishfield and Dr. Takuya Nakanowatari for their collaboration and advice. We also thank Dr. Trudi Semeniuk and David MacDonald, MSc, from Edanz Group for editing drafts of this manuscript.

REFERENCES

Cavalieri, D.J., P. Gloersen and W. J. Campbell (1984): Determination of sea ice parameters with the NIMBUS 7 SMMR, *J. Geophys. Res.*, **89**(D4), 5355–5369.

Comiso, J. C., and F. Nishio (2008): Trends in the sea ice cover using enhanced and compatible AMSR-E, SSM/I, and SMMR data, J. *Geophys. Res.*, **113**, C02S07, doi:10.1029/2007JC004257.

Drucker, R., S. Martin, and R. Moritz (2003): Observation of ice thickness and frazil ice in the St. Lawrence Island polynya from satellite imagery, upward looking sonar, and salinity/temperature moorings, *J. Geophys. Res.*, **108**(C5), 3149, doi:10.1029/2001JC001213.

Giles, K. A., S. W. Laxon, and A. L. Ridout (2008): Circumpolar thinning of Arctic sea ice following the 2007 record ice extent minimum, *Geophys. Res. Lett.*, **35**, L22502, doi:10.1029/2008GL035710.

Krishfield, R. A., A. Proshutinsky, K. Tateyama, W. J. Williams, E. C. Carmack, F. A. McLaughlin and M.-L. Timmermans (2014): Deterioration of perennial sea ice in the Beaufort Gyre from 2003 to 2012 and its impact on the oceanic freshwater cycle, *J. Geophys. Res.*, **119**(2), 1271–1305.

Kwok, R., Cunningham, G., Zwally, H., and Yi, D. (2007): Ice, Cloud, and land Elevation Satellite (ICESat) over Arctic sea ice: retrieval of freeboard, *J. Geophys. Res.*, **112**, C12013, doi:10.1029/2006JC003978.

Kwok, R., G. F. Cunningham, N. LaBell-Hamer, B. Holt, and D. A. Rothrock (1999): Sea ice thickness from high-resolution SAR imagery, *Eos Trans. AGU*, **80**, 495–497.

Laxon, S. W. and 14 co-authors (2013): CryoSat-2 estimates of Arctic sea ice thickness and volume, *Geophys. Res. Lett.*, **40**, 732–737, doi:10.1002/grl.50193.

Polashenski, C., D. K. Perovich, J. A. Richter-Menge, B. Elder (2011): Seasonal Ice Mass-Balance Buoys: Adapting tools to the changing Arctic. *Ann. Glaciol.*, **52** (57), 18-26.

Richter-Menge, J. A., et al. (2006): Ice mass balance buoys: A tool for measuring and attributing changes in the thickness of the Arctic sea ice cover, *Ann. Glaciol.*, **44**, 205 – 210.

Ricker, R., Hendricks, S., Helm, V., Skourup, H., and Davidson, M. (2014): Sensitivity of CryoSat-2 Arctic sea-ice freeboard and thickness on radar-waveform interpretation, *The Cryosphere*, **8**, 1607–1622, doi:10.5194/tc-8-1607-2014.

Tamura, T., K. I. Ohshima, and S. Nihashi (2008): Mapping of sea-ice production for Antarctic coastal polynyas. *Geophys. Res. Lett*. **35**, L07606.

Yu, Y. and D. A. Rothrock (1996): Thin ice thickness from satellite thermal imagery, *J. Geophys.Res.*, **101**, 25,753-25,766.